AALTO UNIVERSITY
SCHOOL OF ELECTRICAL ENGINEERING

Ravi Sundaria

3-D Eddy Current Modelling of Laminations to Study Edge Effects

Thesis submitted for examination for the degree of Master of Science in Technology.
Espoo 25.1.2016

Thesis supervisor:

Professor Antero Arkkio

Thesis instructor:

Assistant Professor Paavo Rasilo (TUT)

Author: Ravi Sundaria

Title: 3-D Modelling of Eddy Currents in Laminations to Study Edge Effects

Date: 30.11.2015 Language: English Number of pages: 7+47

Department of Electrical Engineering and Automation

Professorship: Electromechanics Code: S-17

Supervisor: Professor Antero Arkkio

Instructor: Assistant Prof. Paavo Rasilo (TUT)

This thesis deals with analysis of eddy current losses in steel laminations and shows comparative study of 1-D coupled 2-D loss model with 2-D coupled 3-D loss model. Primary objective of the thesis is to analyze the edge effects in eddy current loss modelling which are ignored in traditionally available 1-D coupled 2-D loss models. Two separate cases, one with homogeneous and second with non-homogeneous flux density distribution across lamination were analyzed. For 1-D homogeneous case eddy current loss model was simulated using MATLAB while in house software FCSMEK was utilized in calculating 2-D eddy current losses in non-homogeneous flux distribution in a salient pole synchronous machine rotor pole. Lamination thickness of 2 mm used in synchronous machine rotor at industrial level to reduce manufacturing costs may have high edge effects and necessitates the requirement to carry out this thesis work.

3-D models of laminations are made with the help of softwares COMSOL and GMSH and FEM calculations are performed in software ELMER. The boundary conditions of 3-D model were excited from field solution of respective 2-D model. As a result of this thesis considerable amount of deviation in eddy current losses has been observed specially at higher thicknesses of steel laminations and frequency of flux density in both homogeneous and non-homogeneous cases.

Keywords: Electrical Machines, Finite Element Method (FEM), Eddy Currents, Steel Laminations

Acknowledgement

This thesis work was carried out at Aalto University, Finland in the department of Electrical Engineering and Automation between May 2015 and November 2015. I would like to thank my supervisor Prof. Antero Arkkio for giving me this opportunity to work under him and do this research. This thesis work can not be completed without the regular guidance from my instructor Assistant Prof. Paavo Rasilo who was providing an active support even during his new job responsibilities at Tampere University of Technology and guided me through each and every step of this thesis.

I would like to thank Prof. Anouar Belachen for regular suggestions and proactively organizing meetings at CSC Finland for ELMER consultation. Many useful discussions with Bishal, Antti, Sabin, Vicente and other colleagues from electromechanics laboratory helped me to move forward in this challenging journey and provided a nice working environment. I would also like to express my gratitude to Mr. Ari Havisto for arranging all the technical resources required for this thesis.

Finally, I would like to thank my parents and other family members for giving moral support during these months. I also express my gratitude to Jay and friends at Aalto University for making the stay enjoyable.

Otaniemi, 30.11.2015

Ravi Sundaria

Table of Contents

List of Figures

List of Symbols and Abbreviation

Symbols

$\boldsymbol{A}$	Magnetic vector potential
$\boldsymbol{AV}$	Vector function for Whitney element
$\boldsymbol{B}$	Magnetic flux density
$\boldsymbol{B}_0$	Average magnetic flux density
$\boldsymbol{B}_\mathrm{p}$	Peak magnetic flux density
c	Experimental iron-loss coefficient
d	Lamination thickness
$\boldsymbol{D}$	Electric flux density
$\boldsymbol{E}$	Electric field strength
F_sk	Skin effect factor
f_s	Supply frequency
$\boldsymbol{H}$	Magnetic flux intensity
$\boldsymbol{H}_\mathrm{s}$	Surface magnetic flux intensity
$\boldsymbol{J}$	Current density
$\boldsymbol{J}_\mathrm{s}$	Source current density
k	Material constant
N_b	Number of basis functions
N_z	Number of integration points
P	Iron loss coefficients
P_J	Eddy current loss with skin effect
$\boldsymbol{T}$	Current vector potential
w/d	Width to thickness ratio of lamination
α	Analytical Iron loss coefficient
β	Analytical iron loss coefficient
δ	Skin depth
η	Weight function in FEM
μ	Permeability of material
ϑ	Reluctivity of material
ρ	Electric charge density

σ	Conductivity of material
Ω	Domain for FEM
ω	Angular frequency

Abbreviations

1-D	One dimensional
2-D	Two dimensional
3-D	Three dimensional
FEM	Finite element method
HVAC	Heating ventilation and air conditioning

1. Introduction

1.1 Background

Electrical machines are integral part of modern industry. It is shown that about 40 percent of electrical energy is consumed by electrical motors and a vital role is played in electricity production by generators. Therefore efficient machines are necessity for sustainable future of the world.

At generation level, electrical generators are traditional conversion devices from fossil fuels to electrical energy. With advent of renewable energy sources like hydro, wind and tidal energy, electrical generators will continue to play dominating role in electrical power generation. Nearly every generation resource utilizes electrical generators to produce electrical energy from the respective fuel source.

At the application level, industry utilizes electrical motors at wide scale. We have seen typical uses of motors in HVAC (heating ventilation and air conditioning), conveyor systems, robotic, machining etc. Low power motors are widely used at households as various domestic appliances. Increasing energy demand of electricity is further translating in ever increasing usage of electrical motors. New fields such as electrical vehicles and industrial automation are shaping future market for novel electrical motors.

As the usage of machines is increasing every passing year, governments around the world are also adopting high energy efficiency regulations for electrical generators and motors. According to European Commission Regulation by 2017 electrical motor with rated output 0.75 -375 kW must meet either IE3 efficiency level or IE2 if fitted with variable frequency drives [1]. These regulations further create requirement to develop more energy efficient machines in future.

To meet the challenge of developing efficient motors, engineers often face challenges in predicting losses in electrical machines with higher accuracy. These losses can be broadly divided in mechanical and electrical losses. Mechanical losses can be seen as friction and windage, while electrical losses can be further divided in ohmic losses in windings, stray-load losses and core losses. Among electrical losses, Iron losses contribute significant part and accurate prediction of these losses remains a challenging research field.

Further, for analysis purpose, computational resources are being extensively used in performing numerical simulations. Finite element analysis is performed in the field of

electrical machines from past few decades to carry out these simulations. As the computational capabilities are increasing day by day, more advanced tools are used for the analysis. As a result, three dimensional finite element analysis is now becoming popular and providing platform for simulating more complex and realistic phenomena in the field of loss estimation and electrical machine design.

This thesis primarily studies the salient pole synchronous machines in respect to eddy current losses in rotor laminations. Salient pole synchronous machines are in use from past hundred years and main utilization of these machines are in low speed applications such as hydroelectric generators, ship propulsion, and rolling mills etc.[2,3]. The rotor of these machines is excited by direct current supply and fundamental rotor flux does not induce eddy current losses in the rotor core. Therefore relatively thick laminations are used in rotor to reduce the manufacturing cost. However due to rotor saliency and stator slotting, harmonics are induced in airgap flux density and cause eddy currents at pole edges [4].

For the above mentioned reasons the work in the direction of modelling eddy current losses in laminations began in mid-nineties. 1-D and 2-D eddy current loss models are first developed and used extensively for this purpose. However considering the limitation of modelling edge effects and 3-D nature of eddy current, requirement of 3-D modelling was felt by researchers. Initial work in 3-D modelling has begun in late nineties and various eddy current formulations were presented [5, 6]. As the high computational burden of simulating a complete system proves to be critical, a 2-D coupled analysis is used in the thesis to simulated 3-D model. Similar work has been shown in [7] for induction machine laminations. Moreover considering the thick laminations of synchronous machines rotor eddy current losses are proved to be major contributors in core losses of this particular machine type.

1.2 Aim of the thesis

This project deals with the study of eddy currents in laminations. The study is based on the coupling of 2-D finite element analysis solution of the machine and 3-D model of lamination. Various lamination thicknesses are considered to evaluate the losses from 2-D and 3-D analysis.

The primary objectives of the thesis are as follows

- Literature review of 1-D, 2-D, 3-D eddy current formulations
- Literature review of various existing 3-D eddy current formulations for laminations
- Computation of 2-D field solution of the machine under study with help of in-house finite element software.

- Development of 3-D lamination model and simulation with help of open source softwares.
- Comparative study and analysis of 1-D coupled 2-D and 2-D coupled 3-D eddy current losses.
- Write a comprehensive thesis report based on computations, solutions and comparisons among used techniques.

1.3 Structure of the thesis

The Thesis is divided into five chapters. The current chapter deals with a brief overview of the thesis and motivation of the work. Further main objectives are explicitly stated to emphasize the contributions of the work.

Second chapter, describes the relevant literature in eddy current loss modelling. Starting from basic finite element formulations, 1-D, 2-D and 3-D eddy current loss models are discussed. Special attention has been given on 3-D loss models.

In third chapter, 1-D eddy current loss model is evaluated for different thickness and frequencies. Further, 2-D FEM simulations are carried on salient pole synchronous machine for a given loading condition with help of software FCSMEK which is developed at the department of Electrical Engineering and Automation, Aalto University. The respective results are discussed in detail.

Fourth chapter deals with 3-D model preparation in open source finite element analysis softwares ELMER, GMSH and PARAVIEW for rotor and cuboid laminations. Further details of eddy current losses are emphasized over range of lamination thickness.

Final chapter discusses the comparative study of computed 1-D coupled 2-D and 2-D coupled 3-D eddy current losses and draws conclusions. A brief description of future work in the area is also suggested.

2. Literature Review

Eddy currents are induced in a conducting body when it is exposed to time varying magnetic fields. As the rate of change of magnetic fields increases the corresponding eddy current losses also increase. The direction of these eddy currents follow the fundamental law of magnetic induction which is popularly known as Lenz law. According to this law eddy currents will oppose the change in magnetic field.

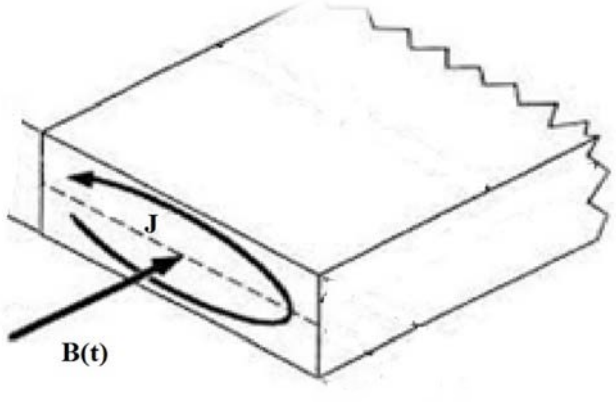

Figure 2.1 Eddy currents in a conductor

2.1 Analytical methods for core losses

The work in the direction of core loss computation in the laminations has begun in late nineteenth century. Initial work was started by Steinmetz (1892) [8], who examined the effects of unidirectional and sinusoidal alternating flux in ferromagnetic laminations. His experimental results predicted that iron losses in laminations are proportional to power of peak magnitude of magnetic flux density and fundamental supply frequency.

$$P_{\mathrm{Fe}} = kB_{\mathrm{p}}^{\alpha} f_{\mathrm{s}}^{\beta} \tag{2.1}$$

Here k, α and β are the constants based on the experimental data. Further B_{p} is peak value of magnetic flux density and f_{s} is supply frequency. Over the period of time this expression has undergone several changes and Bertotti provided three components of

iron losses named as hysteresis loss, classical eddy current loss and excess loss. These components are expressed as

$$P_{\text{ex}} = c_{\text{hy}} f_{\text{s}} B_{\text{p}}{}^{2} + c_{\text{cl}} f_{\text{s}}{}^{2} B_{\text{p}}{}^{2} + c_{\text{ex}} f_{\text{s}}{}^{1.5} B_{\text{p}}{}^{1.5} \tag{2.2}$$

Hysteresis loss $P_{\text{hy}} = c_{\text{hy}} f_{\text{s}} B_{\text{p}}{}^{2}$

Classical eddy current loss $P_{\text{cl}} = c_{\text{cl}} f_{\text{s}}{}^{2} B_{\text{p}}{}^{2}$

Excess loss $P_{\text{ex}} = c_{\text{ex}} f_{\text{s}}{}^{1.5} B_{\text{p}}{}^{1.5}$

The parameters c_{hy}, c_{cl} and c_{ex} depend on the material properties of lamination. Hysteresis losses are caused from the hysteretic nature of ferromagnetic material, classical eddy current losses account the losses due to eddy currents when domain structure of material has not been considered and excess losses represent microscopic eddy current loss caused by domain wall movement. Hysteresis energy losses are static in nature however classical and excess losses depend on the rate of change of magnetic flux density. The coefficient of classical eddy current loss for a lamination having a uniform flux density over the thickness d and conductivity σ is calculated as

$$c_{\text{cl}} = \frac{\sigma d^{2} \pi^{2}}{6} \tag{2.3}$$

The coefficients c_{hy} and c_{ex} are calculated based on measurements with different amplitudes and frequencies of sinusoidal alternating flux densities. Further, eddy current losses can be modified with inclusion of skin effect [9]. The skin effect factor can be calculated as

$$F_{\text{sk}} = \frac{3}{\lambda} \frac{\sinh \lambda - \sin \lambda}{\cosh \lambda - \cos \lambda} \tag{2.4}$$

Further, the skin effect factor depends on the ratio $\lambda = \frac{d}{\delta}$, which is function of lamination thickness d and frequency dependent skin depth δ. The skin depth can be calculated as $\delta = \sqrt{\frac{1}{\pi f_{\text{s}} \sigma \mu}}$ and depends on the material properties and frequency of magnetic flux density. Here μ represents permeability of the lamination material. Finally the analytical expression for eddy current loss in a lamination with linear material can be represented by equation 2.5.

$$P_{\text{J}} = c_{\text{cl}} f_{\text{s}}{}^{2} B_{\text{p}}{}^{2} F_{\text{sk}} \tag{2.5}$$

2.2 Finite element method in electromechanics

Finite element technique is a numerical analysis tool which is popular in engineering streams from past few decades. Use of finite element analysis in electrical machine design nurtured a way towards accurate field calculations. Complex geometries and nonlinearities of materials are modeled successfully through FEM. This proves to be a major advantage in comparison with traditionally existed analytical methods. Earlier circuit coupled equations are solved with 2-D finite element analysis for evaluation of electrical machines [10]. With the advent of computational capacity, 3-D FEM techniques are also becoming popular nowadays.

The basic physical laws governing the problem formulation in finite element analysis are as follows

- Gauss law –
  According to this law total electric charge inside a closed volume represents the total electric flux coming out from the surfaces.

$$\nabla \cdot \boldsymbol{D} = \rho \tag{2.6}$$

$$\oint_s \boldsymbol{D} \cdot ds = \oint_v \rho dv \tag{2.7}$$

- Gauss magnetism law
  Magnetic flux flows in a close loop and the divergence of magnetic flux density is always zero. In other words magnetic monopole does not exist in nature.

$$\nabla \cdot \boldsymbol{B} = 0 \tag{2.8}$$

$$\oint_s \boldsymbol{B} \cdot ds = 0 \tag{2.9}$$

- Faraday law
  Faraday law represents the relation of time varying magnetic field with electric field.

$$\nabla \times \boldsymbol{E} = -\frac{\partial \boldsymbol{B}}{\partial t} \tag{2.10}$$

$$\oint_L \boldsymbol{E} \cdot dl = -\oint_s \frac{\partial \boldsymbol{B}}{\partial t} \cdot ds \tag{2.11}$$

- Ampere law
  According to this law flow of current in a conductor gives rise to magnetic field which encircles the current. Displacement current term is added by Maxwell in Ampere circuital law to include the effect of magnetic field generated by time varying electric field and dielectric polarization.

$$\nabla \times \boldsymbol{H} = \boldsymbol{J} + \frac{\partial \boldsymbol{D}}{\partial t} \tag{2.12}$$

In electromechanical problems generally current density $\boldsymbol{J}$ is much larger than the displacement current $\frac{\partial \mathbf{D}}{\partial t}$. Therefore displacement current term is neglected.

$$\nabla \times \boldsymbol{H} = \boldsymbol{J} \tag{2.13}$$

$$\oint_L \boldsymbol{H} \cdot dl = \oint_s \boldsymbol{J} \cdot ds \tag{2.14}$$

- Material equations
  The magnetic and electrical quantities expressed above are related to each other from material specific properties.

$$\boldsymbol{B} = \mu \boldsymbol{H} \tag{2.15}$$
$$\boldsymbol{H} = \vartheta \boldsymbol{B} \tag{2.16}$$
$$\boldsymbol{J} = \sigma \boldsymbol{E} \tag{2.17}$$

Here μ is permeability, σ is conductivity and ϑ is known as reluctivity of the material. These quantities need not to be simple constants and these values are functions of magnetic and electric fields.

The main idea of finite element method is to approximate the function involved in the problem by simple expressions within each finite element. First the problem region is divided into many small regions which are known as finite elements. Then we define the points where required field quantity needs to be computed, these points are called as nodal points. However in case of edge elements we focus on elemental fields rather than nodal field due to solution procedure in three dimensional space. Later shape functions are chosen in such a fashion that the value of a shape function is unity for the corresponding node and zero at all other nodes. Further, these shape functions are combined to form global shape function which is also sometimes known as basis function. Number of nodes and shapes of a finite element determine the behavior of shape functions. A sample triangular first order mesh (nodes only at the vertices) is shown in figure 2.2.

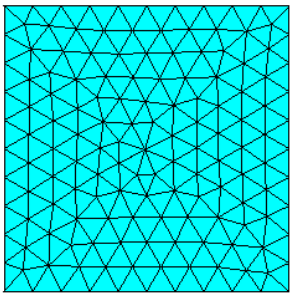

Figure 2.2 First order triangular finite element mesh

A sample example of shape functions can be taken from Langrange interpolation in case of a triangular mesh. As shown in the figure 2.3 below, a first order triangular element has three nodes which are positioned at vertices of the triangle.

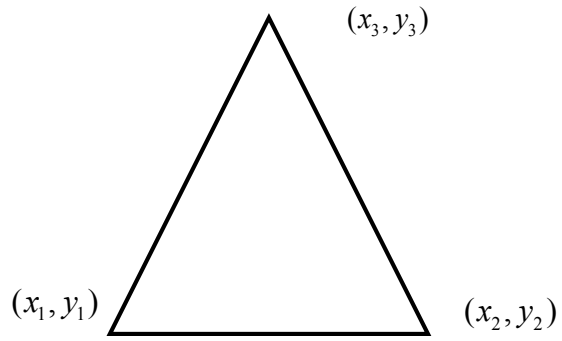

Figure 2.3 A sample triangular element

$$N_1 = \frac{(x-x_2)(x-x_3)}{(x_1-x_2)(x_1-x_3)} \tag{2.18}$$

$$N_2 = \frac{(x-x_1)(x-x_3)}{(x_2-x_1)(x_2-x_3)} \tag{2.19}$$

$$N_3 = \frac{(x-x_2)(x-x_1)}{(x_3-x_2)(x_3-x_2)} \tag{2.20}$$

N_1, N_2, N_3 are the shape functions corresponding to the points $(x_1, y_1), (x_2, y_2), (x_3, y_3)$. Method of weighted residuals is applied by use of scalar or vector potential of desired field quantity (u) and above mentioned Maxwell equations. We finally arrive at generalized Poisson equation, which is represented as

$$\nabla \cdot (k \nabla u) + g = 0 \tag{2.21}$$

Here u is the field quantity we are solving; k and g are functions of position. According to method of weighted residuals the equation (2.21) needs to be satisfied at each point in the region. The following expression is obtained by multiplying the equation (2.21) by a weight function η and integrating it over the whole domain Ω.

$$R = \int_{\Omega} \eta \left[\nabla \cdot (k \nabla u) + g \right] d\Omega = 0 \tag{2.22}$$

The solution of above equation depends on the choice of weight function η and shape functions are used to approximate u. In practice the selection of weight function η is done by Galerkin method and shape functions are used as weight functions. Finally we arrive at matrix equation

$$S\boldsymbol{a} = \boldsymbol{f} \tag{2.23}$$

Here stiffness matrix S and vector $\boldsymbol{f}$ is represented as a function of shape functions

$$S_{ij} = \int_{\Omega} k \left(\nabla N_i \right) \cdot \left(\nabla N_j \right) d\Omega \tag{2.24}$$

$$\boldsymbol{f} = \int_{\Omega} g N_i d\Omega \tag{2.25}$$

In case of time derivative magnetic field the mentioned unknown variable $\boldsymbol{a}$ also changes with time and equation (2.23) can be modified as

$$S\boldsymbol{a} + T \dot{\boldsymbol{a}} = \boldsymbol{f} \tag{2.26}$$

Above equation requires time and space discretization for further numerical solution. Problem domain can be represented as a mesh which contains several elements. Generally in 2-D, triangles and rectangles and in 3-D, prism, tetrahedral and hexahedral elements are used. For every geometry, shape functions are expressed in local coordinates as shown in equations (2.18-2.20). The coordinate transformation between the local and global xyz space is achieved with the help of isoparametric elements. If local coordinate system is represented by $\xi\eta\zeta$ space then global coordinates can be shown as

$$x = \sum_{j=1}^{n} N_j \left(\xi, \eta, \zeta \right) x_j \tag{2.27}$$

$$y = \sum_{j=1}^{n} N_j \left(\xi, \eta, \zeta \right) y_j \tag{2.28}$$

$$z = \sum_{j=1}^{n} N_j \left(\xi, \eta, \zeta \right) z_j \tag{2.29}$$

After discretization, the resulting equations are solved with the help of direct and iterative methods. For small problems direct methods such as Gaussian elimination,

Triangular decomposition and Cholesky's method are used. However iterative methods like Gradient and Conjugate Gradient methods are preferred for solving relatively larger systems. The convergence of iterative algorithms can be accelerated with the support of preconditioning methods. The permeability of the iron in electrical machine shows nonlinear behavior and therefore creates a set of nonlinear equations. These nonlinear equation sets are better solved by Newton-Raphson method in the software used for 3-D computation.

In general electromagnetics time dependent first order derivative equations are discretized with help of various methods. Under this thesis work Crank Nicolson method was applied in FCSMEK for 2-D time step analysis of salient pole synchronous machine and first order backward difference formula was used for time discretization in ELMER.

- Crank-Nicolson Method
  As per Crank-Nicolson method, at time step t_{k-1} the vector of nodal values $\boldsymbol{a}^{k-1}$ is known then solution for $\boldsymbol{a}^{k}$ are required to be computed at time step $t_k = t_{k-1} + \Delta t$

  Mentioned nodal variable is approximated as $\frac{1}{2}\left(\dot{\boldsymbol{a}}^{k} + \dot{\boldsymbol{a}}^{k-1}\right) = \frac{\boldsymbol{a}^{k} - \boldsymbol{a}^{k-1}}{\Delta t}$ and equation (2.26) can be written at time step t_k as

$$S\boldsymbol{a}^{k} + T\left[\frac{2}{\Delta t}\left(\boldsymbol{a}^{k} - \boldsymbol{a}^{k-1}\right) - \dot{\boldsymbol{a}}^{k-1}\right] = \boldsymbol{f}^{k} \tag{2.30}$$

  Finally we arrive at algebraic equation in the form of

$$\left(S + \frac{2}{\Delta t}T\right)\boldsymbol{a}^{k} = -\left(S + \frac{2}{\Delta t}T\right)\boldsymbol{a}^{k-1} + \boldsymbol{f}^{k} + \boldsymbol{f}^{k-1} \tag{2.31}$$

- Backward Difference Formulae (BDF) of several order [11]
  This type of time discretization method is extensively used in finite element software ELMER. BDF of several orders are listed in ELMER manual and under this thesis BDF order one has been used for time discretization. Backward difference formula of first order is expressed as

$$\left(S + \frac{1}{\Delta t}T\right)\boldsymbol{a}^{k} = \left(\frac{1}{\Delta t}T\right)\boldsymbol{a}^{k-1} + \boldsymbol{f}^{k} \tag{2.32}$$

2.3 Edge elements or Whitney elements and characteristics

In 3-D, the required vector quantities have three components and nodal elements should describe the respective three components. Under such conditions edge elements have natural advantage as these type of finite elements have a vector character [12]. A vector function is approximated by linear summation of shape functions of respective edges in each edge finite element. Within an element the vector function $\boldsymbol{AV}$ is approximated as

$$\boldsymbol{AV} = \sum_{i=1}^{n} AV_{ti}\boldsymbol{N}_{ni} \tag{2.33}$$

Here the coefficient AV_{ti} is the degree of freedom at edge i and $\boldsymbol{N}_{ni}$ is the edge shape function related to edge i. The index n represents the total number of edges in the edge finite element under consideration. For example, for a tetrahedral mesh n=6 and similarly the value of n for a hexahedral mesh will be 12. In contrast to 2-D nodal finite elements where the value of shape function is unity at the corresponding node, in edge elements the value of line integral of a shape function with respective edge will attain unity value.

$$\int_i \boldsymbol{AV}.dl = \int_i AV_{ti}\boldsymbol{N}_{ni} \cdot d\boldsymbol{l} = AV_{ti} \tag{2.34}$$

Hence, AV_{ti} is the line integral of $\boldsymbol{AV}$ along edge i and in edge elements, the degree of freedom is the line integral of the approximated vector function along the edge instead of components of vector function in nodal elements.

In case of two elements share an edge, the degree of freedom of vector field line integral at that edge are set to be equal. The same is applicable throughout the domain and makes the vector function tangentially continuous across all element interfaces. On the other hand the vector function is not normally continuous. The mapping of local to global coordinates system is done in a similar way as described in equations (2.27-2.29).

In early 1980's, Nedelec presented some types of three dimensional finite elements and one of the type was edge element [13]. Later on Bossavit developed tetrahedral shape functions and delivered a method for constructing Whitney forms applied to several types of finite elements [14]. Wang and Ida described curvilinear and higher order edge elements for more complex geometries and fine field computations [15]. Advantage of using edge elements in case of sharp edges are discussed by Webb [16]. However in complicated geometries higher order elements may not be a best choice in all cases and a high-density first order mesh can give better result. In this thesis first order prism elements and tetrahedral elements are primarily considered for 3-D computations.

2.4 Eddy current formulation

As described earlier time dependent fields which are responsible for eddy currents inside a lamination, are modelled with the help of Maxwell equations. The basis of calculation of eddy current are presented by equations

$$\nabla \times \boldsymbol{E} = -\frac{\partial \boldsymbol{B}}{\partial t} \tag{2.35}$$

$$\nabla \times \boldsymbol{H} = \boldsymbol{J} \tag{2.36}$$

Material laws are used to arrange the above mentioned equations in a form of differential equation of a physical quantity. With the help of ohm law $\boldsymbol{J}=\sigma\boldsymbol{E}$, where σ is the conductivity of medium, we get

$$\nabla \times \nabla \times \boldsymbol{H} = \sigma \nabla \times \boldsymbol{E} \tag{2.37}$$

$$\nabla \times \nabla \times \boldsymbol{H} = -\sigma \frac{\partial \boldsymbol{B}}{\partial t} \tag{2.38}$$

The above equation represents general quasistatic eddy current problem for flux density $\boldsymbol{B}$ and field strength $\boldsymbol{H}$ in a medium. $\boldsymbol{H}$ and $\boldsymbol{B}$ are dependent on the position and time.

2.4.1 1-D formulation

As explained in [17], eddy currents can be treated by 1-D diffusion equation if return path of eddy currents (component along the lamination thickness) are neglected. If the rolling surface is in *xy* plane, then respective lamination thickness will be in *z* direction. The 2-D finite element solution provides the magnetic flux density in each element of the mesh and as *z* component of induced currents are neglected, the corresponding eddy current distribution can be evaluated.

$$\frac{\partial^2 \boldsymbol{H}_{xy}(z,t)}{\partial z^2} = \sigma \frac{\partial \boldsymbol{B}_{xy}(z,t)}{\partial t} \tag{2.39}$$

Here *xy* refer to one position in the plane related to specific 2-D mesh element and field quantities are computed only in *z* direction. Further magnetic field strength and flux density are shown as

$$\boldsymbol{H}_{xy} = H_x \boldsymbol{u}_x + H_y \boldsymbol{u}_y \tag{2.40}$$

$$\boldsymbol{B}_{xy} = B_x \boldsymbol{u}_x + B_y \boldsymbol{u}_y \tag{2.41}$$

A simple 1-D iron loss model was considered which takes average magnetic flux density as an input and calculates surface field strength as shown in [18]. Electrical

conductivity σ is assumed constant. The model further approximates the magnetic flux density distribution along the thickness $z \in [-d/2, d/2]$ by Fourier cosine series with N_b basis function as

$$\boldsymbol{B}(z,t) = \sum_{n=0}^{N_b-1} \boldsymbol{B}_n(t)\alpha_n(z) \tag{2.42}$$

, $\alpha_n(z) = \cos\left(2n\pi\frac{z}{d}\right)$. Cosine functions have been chosen. These functions lead the spatial average flux density in the lamination to the average flux density ($\boldsymbol{B}_0$). Further, field strength is approximated as

$$\boldsymbol{H}(z,t) = \boldsymbol{H}_s(t) - \sigma d^2 \sum_{n=0}^{N_b-1} \frac{\partial \boldsymbol{B}_n(t)}{\partial t}\beta_n(z) \tag{2.43}$$

Here $\boldsymbol{H}_s$ is surface magnetic field strength. This approximation satisfies equation (2.39) provided

$$\alpha_n(z) = -d^2\frac{\partial^2\beta_n(z)}{\partial z^2} \tag{2.44}$$

β_n is defined as $\beta_n(\pm d/2) = 0$.

Integrating the equation (2.43) along the thickness leads to system of equations

$$\begin{bmatrix} \boldsymbol{H}_s \\ 0 \\ \vdots \end{bmatrix} = \frac{1}{d}\int_{-d/2}^{d/2} \boldsymbol{H}(z,t)\begin{bmatrix} \alpha_0(z) \\ \alpha_1(z) \\ \vdots \end{bmatrix} dz + C\frac{\partial}{\partial t}\begin{bmatrix} \boldsymbol{B}_0(t) \\ \boldsymbol{B}_1(t) \\ \vdots \end{bmatrix} \tag{2.45}$$

The elements of matrix C are obtained from integration over the lamination thickness as

$$C_{mn} = \sigma d^2\left(\frac{1}{d}\int_{-d/2}^{d/2}\alpha_m(z)\beta_n(z)dz\right) \tag{2.46}$$

The local eddy current loss density (W/m^3) is calculated from electric field strength E_{xy} as

$$P_{cl}(z,t) = \sigma E^2{}_{xy}(z,t) \tag{2.47}$$

Further, with the help of Farady law $\nabla \times \boldsymbol{E}(z,t) = \frac{-\partial \boldsymbol{B}(z,t)}{\partial t}$ eddy current loss density can be represented in equation 2.48.

$$P_{\mathrm{cl}}(z,t) = \sigma\left(\int \frac{\partial \boldsymbol{B}(z,t)}{\partial t} dz\right)\cdot\left(\int \frac{\partial \boldsymbol{B}(z,t)}{\partial t} dz\right)$$
$$= \sigma \sum_{m=0}^{N_{\mathrm{b}}-1} \sum_{n=0}^{N_{\mathrm{b}}-1} \frac{\partial \boldsymbol{B}_m(t)}{\partial t}\cdot\frac{\partial \boldsymbol{B}_n(t)}{\partial t} \int \alpha_m(z)dz \int \alpha_n(z)dz \tag{2.48}$$

Finally, the average power loss density over a full cycle can be obtained as shown in equation 2.49.

$$P_{\mathrm{cl}}(z) = \frac{1}{T}\int_T P_{\mathrm{cl}}(z,t)dt \tag{2.49}$$

2.4.2 1-D coupled 2-D formulation

The presented 1-D eddy current loss model needed to be coupled with the 2-D finite element model of electrical machine. As presented in [18], the 1-D model is included in 2-D field solution by applying Ampere's law to the surface field strength. We can assume symmetry across the laminations which lead to the condition of zero normal current density at the parallel surfaces of the lamination.

$$\nabla_{xy} \times \boldsymbol{H}_{\mathrm{s}}(x,y,t) = \left(\frac{\partial H_{\mathrm{s},y}(x,y,t)}{\partial x} - \frac{\partial H_{\mathrm{s},x}(x,y,t)}{\partial y}\right)\boldsymbol{u}_z = 0 \tag{2.50}$$

The representation of del operator ∇_{xy} shows application in *x*-*y* plane only. Further, the magnetic flux density can be represented by magnetic vector potential to satisfy the Gauss law of magnetism. Finally the curl operator is applied to equation (2.45) to get the total system of equation for a 2-D lamination model as presented in equation (2.51).

$$\frac{1}{d}\nabla_{xy} \times \int_{-d/2}^{d/2} \boldsymbol{H}(z,t)\begin{bmatrix}\alpha_0(z)\\ \alpha_1(z)\\ \vdots\end{bmatrix}dz + C\nabla_{xy} \times \frac{\partial}{\partial t}\begin{bmatrix}\boldsymbol{B}_0(x,y,t)\\ \boldsymbol{B}_1(x,y,t)\\ \vdots\end{bmatrix} = \begin{bmatrix}0\\ 0\\ \vdots\end{bmatrix} \tag{2.51}$$

2.4.3 3-D formulation

In quasistatic eddy current problems the eddy currents are only defined in conducting regions and magnetic field has been defined in both conducting and non-conducting region. From Maxwell equations the time varying field is represented as

$$\nabla \times \boldsymbol{E} = -\frac{\partial \boldsymbol{B}}{\partial t} \tag{2.52}$$

Here the flux density can be shown in form of vector potential as

$$\boldsymbol{B} = \nabla \times \boldsymbol{A} \tag{2.53}$$

An extensive summary of various formulations available for eddy current problems is discussed in [6]. The main formulations based on scalar and vector potentials are discussed below.

2.4.3.1 AVA formulation

From equations (2.52-2.53) standard AVA formulations can be obtained as

$$\boldsymbol{E} = -\frac{\partial \boldsymbol{A}}{\partial t} - \nabla V \tag{2.54}$$

In eddy current region

$$\nabla \times \left(\frac{1}{\mu} \nabla \times \boldsymbol{A} \right) + \sigma \frac{\partial \boldsymbol{A}}{\partial t} + \sigma \nabla V = 0 \tag{2.55}$$

Further the divergence free nature of eddy currents can be seen as

$$\nabla \cdot \left(\sigma \frac{\partial \boldsymbol{A}}{\partial t} + \sigma \nabla V \right) = 0 \tag{2.56}$$

In non-conducting region there are no eddy currents and current density in this region is representation of source as shown in equation (2.57).

$$\nabla \times \left(\frac{1}{\mu} \nabla \times \boldsymbol{A} \right) = \boldsymbol{J}_s \tag{2.57}$$

Multiplying the above equations by suitable test function and integrating the same across the whole region will provide an expression suitable for application of Galerkin method and we arrive at required set of equations after proper space and time discretization.

2.4.3.2 TØØ formulation

In this formulation the electric field can be represented as a vector potential and two different representation of electric field vector potential has been used to describe conducting and non-conducting region.

$$\boldsymbol{J} = \sigma \boldsymbol{E} = \nabla \times \boldsymbol{T} + \nabla \times \boldsymbol{T}_o \tag{2.58}$$

Here in conducting region $\boldsymbol{J} = \nabla \times \boldsymbol{T}$ and in non-conducting region $\boldsymbol{J} = \nabla \times \boldsymbol{T}_o$. Further field quantities can be derived in form of potentials as

In conducting region

$$\boldsymbol{H} = \boldsymbol{T}_o + \boldsymbol{T} - \nabla\phi \tag{2.59}$$

In non-conducting region

$$\boldsymbol{H} = \boldsymbol{T}_o - \nabla\phi \tag{2.60}$$

Substitution of potentials into Maxwell equations will form the differential equations to be solved.

In conducting region

$$\nabla\times\left(\frac{1}{\sigma}\nabla\times\boldsymbol{T}\right)+\mu\frac{\partial\boldsymbol{T}}{\partial t}-\mu\nabla\frac{\partial\phi}{\partial t}=-\mu\frac{\partial\boldsymbol{T}_0}{\partial t} \tag{2.61}$$

$$-\nabla\cdot\left(\mu\nabla\phi-\mu\boldsymbol{T}\right)=\nabla\cdot\mu\boldsymbol{T}_o \tag{2.62}$$

And in non-conducting field

$$\nabla\cdot\left(\mu\nabla\phi\right)=\nabla\cdot\mu\boldsymbol{T}_o \tag{2.63}$$

Dirichlet and Neumann boundary conditions on vector and scalar potentials can be applied for parallel flux and current conditions.

2.4.3.3 ATA formulation

As per this formulation, current density is described specifically by current vector potential $\boldsymbol{T}$ and magnetic vector potential $\boldsymbol{A}$ is used to calculate field quantities in the whole domain. Solenoidal nature of $\boldsymbol{B}$ and $\boldsymbol{J}$ on the boundaries is explicitly satisfied by defining tangential component of $\boldsymbol{A}$ and $\boldsymbol{T}$ as Dirichlet conditions. In some cases ATA formulation achieve faster convergence than vector-scalar formulations. Using these potentials in Maxwell equations in conducting region will lead to

$$\nabla\times\left(\frac{1}{\mu}\nabla\times\boldsymbol{A}\right)-\nabla\times\boldsymbol{T}=0 \tag{2.64}$$

$$\nabla\times\left(\frac{1}{\sigma}\nabla\times\boldsymbol{T}\right)+\nabla\times\frac{\partial\boldsymbol{A}}{\partial t}=0 \tag{2.65}$$

Non conducting region is represented as

$$\nabla\times\left(\frac{1}{\mu}\nabla\times\boldsymbol{A}\right)=\boldsymbol{J}_s \tag{2.66}$$

$\boldsymbol{B}$ and $\boldsymbol{J}$ on the boundaries can be specified by the tangential components of $\boldsymbol{A}$ and $\boldsymbol{T}$.

2.4.4 2-D coupled 3-D formulation

As a complete 3-D simulation of electrical machine is computationally expensive for calculation of eddy current losses in laminations, 2-D coupled 3-D models are developed. One such model is presented in [7]. The field simulation is performed by 2-D FEM for the whole machine and vector potential values are obtained at the boundary of laminations. Further 2-D vector potentials are used as source at axial boundaries to enforce average magnetic flux density in the lamination. Proper magnetic insulation conditions along with normal current density values are set at the parallel boundaries to get a unique solution. As 1-D coupled 2-D models neglects the edges, 2-D coupled 3-D model should provide good estimation of edge effects on eddy current losses.

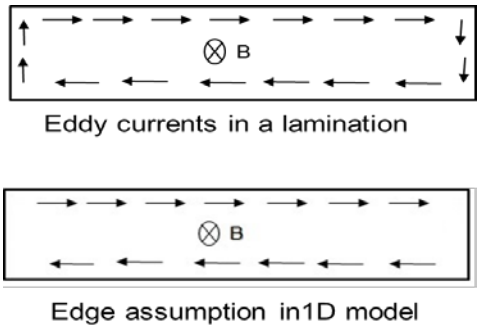

Figure 2.4 Edge assumption in lamination1-D model

3. 2-D FEM Model and Results

The most common way of analyzing electromagnetic field of an electrical machine is 2-D finite element analysis. Magnetic field can be assumed in plane perpendicular to the shaft and machine is represented as cross sectional representation. Major machine properties such as torque – speed characteristics or circuit parameters can be evaluated. The vector potential of magnetic flux density is assumed to have a single component in z direction, provided that the machine cross section is in xy plane.

3.1 Homogeneous flux density case

If we assume a homogeneous flux density distribution across the lamination surface, then a 2-D model can be represented by a single node in 2-D lamination plane. This case facilitates the application of 1-D model described in 2.4.1 by supplying average flux density. MATLAB is used for implementation of this model and number of basis functions and integration points are optimized to give stable results. The input parameters for the model are listed below.

Average magnetic flux density $B_o\,(t) = 1.5 \sin(2\pi f_s t)$
Frequency $f_s = 50$ Hz
Conductivity $\sigma = 8\times10^6$ S/m

Table 3.1 2-D Eddy current losses at 50 Hz

Thickness(mm)	Linear(kW/m^3)	Nonlinear(kW/m^3)
0.20	2.97	2.99
0.50	18.58	19.30
0.65	31.39	33.46
1.00	74.06	83.31
1.50	164.02	196.89
2.00	280.14	360.44
2.25	343.22	460.78
2.50	406.52	573.19

As nowadays electrical motors are fed with variable frequency drives and hence subjected to time varying flux density of frequency of the order kHz. Cases with 1 kHz and 5 kHz has been analyzed and respective eddy current losses are recorded. Further,

nonlinear material characteristics has been specified by single value BH curve (figure 3.1) for all the lamination cases at higher frequencies.

Table 3.2 2-D Eddy current losses at 1000 Hz and 5000 Hz

Thickness (mm)	f_s =1000 Hz (MW/m^3)	f_s =5000 Hz (MW/m^3)
0.50	9.22	239.27
1.50	84.21	1852.30
2.00	144.23	3167.30
2.25	178.75	3946.80
2.50	216.42	4800.60

3.2 Rotor pole of salient pole synchronous machine

Specifically salient pole synchronous machine was selected to analyze edge effects due to the use of thick (2 mm) laminations in rotor pole. As in case of salient pole synchronous generators the rotor field windings produce a DC flux, eddy current losses in rotor pole are assumed to be negligible. Further to reduce the manufacturing cost uninsulated thick rotor laminations are used in commercially available such machines. However eddy currents are induced due to slot harmonics at the rotor pole surfaces. The slot harmonics depend on number of factors such as number of slots in rotor and stator, frequency of supply and type (grid supply or PWM), number of poles, load, airgap length etc. According to the brief literature survey it is found that slot harmonics frequency is in kHz range in rotor frame of reference. Naturally eddy current losses in rotor laminations constitute major portion of iron losses in such type of machines. This can also be clearly seen by iron loss components calculated by 2-D FEM analysis which is presented in table 3.4. The selected machine has four poles with 48 stator slots (Q_s) and fed by 50 Hz grid supply. Under such condition in rotor frame of reference stator slots can be seen at the frequency shown in equation (3.1).

$$F_r = \frac{Q_s f_s}{p} = 1200Hz \tag{3.1}$$

The study of salient pole synchronous machine has been carried out using in-house 2-D finite element software FCSMEK. This machine is designed to work as a low voltage industrial diesel generator and generate rated 50 Hz, 400 V sinusoidal supply at star connected stator terminals. The machine parameters are listed in table 3.3 and magnetization curve of laminated material is shown in figure 3.1.

Table 3.3 Machine Specifications

Parameter	**Value**
Machine type	Generator
Power	150 kVA
Voltage	400 V
Current	217 A
Rated frequency	50 Hz
Number of pole pairs	2
Number of phases	3
Displacement factor	0.8 Cap
Number of conductors in a stator slot	48
Connection	Star
Effective length of the machine	0.146 m
Outer diameter of the stator	430 mm
Inner diameter of the stator	300 mm
Air gap	1.2 mm
Stator lamination	0.5mm,3.0-MS/m Fe-Si sheet

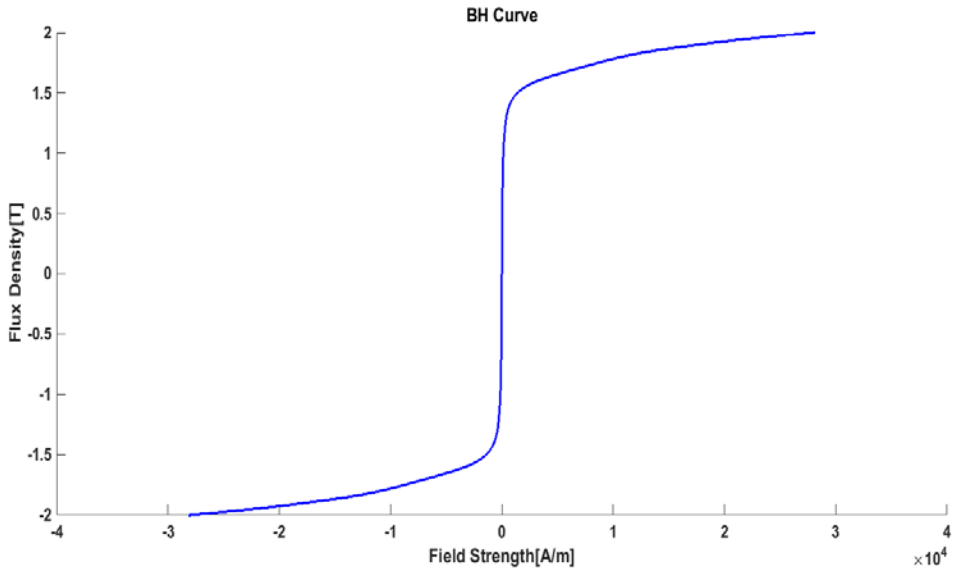

Figure 3.1 B-H curve of lamination material

Rotor pole surface contains eddy currents which are generated by flux density harmonics caused by slot ripples; therefore a relatively large number of time steps are required to successfully model these losses. Under this study Crank-Nicolson method is used for time stepping analysis and two thousand time steps are considered for a period. To avoid the effect of transients, all the simulations are carried out for two periods and field computation along with losses are analyzed for the second period.

As there was a constraint of using first order edge elements in finite element software 'ELMER' for 3-D computation, we have used first order triangular elements for 2-D computation as well. A total of 242 nodes and 362 first order elements are used for the field calculation of front part of the pole. A relatively fine mesh is considered at the pole surface for better calculation of eddy current losses. The 2-D reference mesh is shown in the figure 3.2.

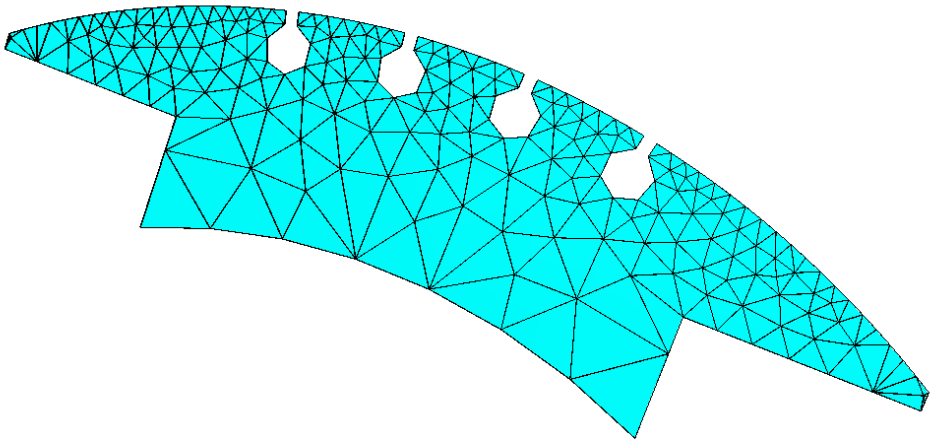

Figure 3.2 2-D Finite element mesh of rotor pole

A complete detail of 2-D FEM solution process in FCSMEK was out of the scope of thesis, therefore only the main results related to the losses will be stressed here after. The main loss components of the machine over a period with twenty five percent loading case are shown below.

Table 3.4 2-D Losses in Machine

Loss type	**Area**	**Value (W)**
Resistive Loss	Stator Winding	307.66
	Damping Cage	68.40
	Rotor Winding	411.83
	Other Conducting Part	141.68
Hysteresis Loss	Stator	618.24
	Rotor	148.25
Eddy Current Loss	Stator	403.45
	Rotor	1894.16
Excess Loss	Stator	187.80
	Rotor	101.85

It can be interpreted from the 2-D loss calculation results that the losses due to eddy currents contribute highest proportion in the total losses at the given loading and supply condition. The field distribution calculated as average value of magnetic flux density

in each first order triangular finite element on the rotor pole can be shown in Figure 3.3.

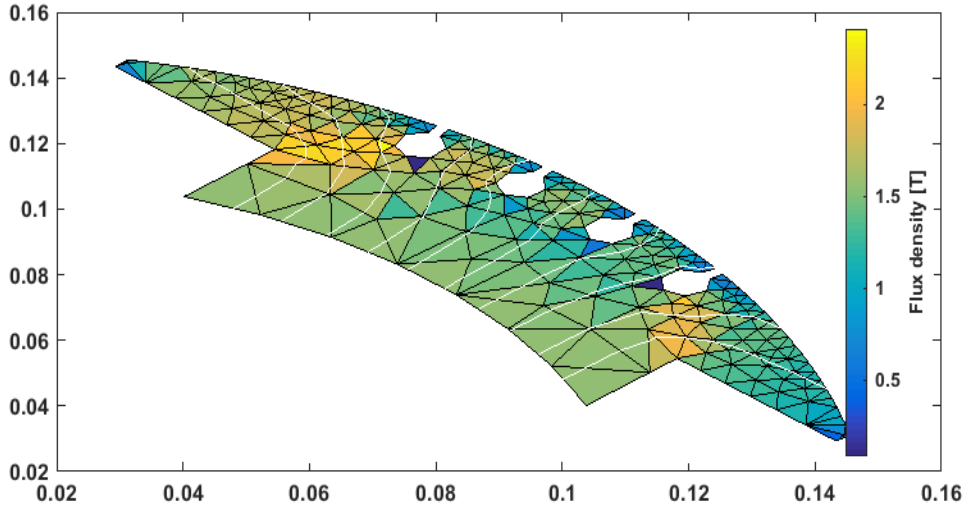

Figure 3.3 Magnetic flux density distribution in pole

The blank round area between the pole represents the damper bars. As the model represents a specific loading condition (not the transient state), no current was assumed in the bars and subsequent meshing for the same has been avoided.

Further, as the main objective of the thesis is the study of edge effects in eddy current loss calculation, a range of lamination thicknesses needs to be taken into consideration. For this purpose we have simulated the given machine with rotor pole lamination thickness as 0.2 mm, 0.35 mm, 0.65 mm, 1 mm and original machine lamination thickness of 2 mm. The 2-D eddy current loss computation results for rotor are presented in table 3.5.

Table 3.5 Eddy current losses at different laminations

Lamination thickness(mm)	**Rotor eddy current loss(W)**
0.20	43.6
0.35	113.92
0.50	207.59
0.65	316.69
1.00	635.48
2.00	1894.16

For the simplistic analysis the value of conductivity is maintained same across all the laminations thicknesses and same as 2 mm steel lamination (σ = 7.85 MS/m) of manufactured rotor.

4. 3-D FEM Model and Results

2-D finite element method for electromechanical analysis of electrical machines was popular since early 1980s. This analysis has obvious advantage of analyzing the machine with respect to providing acceptable accuracy in field calculation using less computational resources as compared to three dimensional analysis. However with advent of more advance computing resources three dimensional analysis is not only becoming more feasible but also successfully adopted to model complex three dimensional physical phenomena such as eddy currents inside a machine. As discussed earlier eddy currents are calculated either by statistical post processing methods or 1-D eddy current models which neglect the edge effects of eddy currents. Therefore to account and analyze these effects with increasing lamination thicknesses 3-D finite element analysis is performed on two test cases, firstly a simple homogenous field distribution on a cuboid lamination and Secondly, on actual rotor of salient pole synchronous machine.

The three dimensional model of lamination is developed in open source multiphysical simulation software ELMER which is developed by CSC-IT center for science, Finland [19]. Elmer has modular structure and each module make computation for a given mesh. For electromechanical field calculation, solver MagnetoDynamics and for computation of derived fields, solver MagnetoDynamicsCalcFields has been used [20]. As this software lacks adequate functionalities for user interface and mesh generation, GMSH and COMSOL have been adopted for creating proper mesh for rotor and cuboid case respectively. Further, for post processing open source software PARAVIEW [21] is used and compatible input files for this software were generated with ELMER module ResultOutputSolve. Eddy current loss calculation at each time step was calculated by separate solver named as SaveData.

As analyzing a whole 3-D model of machine is still computationally burdensome, a 2-D coupled 3-D model of eddy current analysis is adopted for this thesis work. The 3-D model is excited by time dependent boundary conditions derived from a 2-D finite element analysis. AVA eddy current formulation has been applied in this thesis as this formulation was implemented in open source 3-D finite element software ELMER. 2-D vector potential has been imposed on the boundaries of the lamination and due to symmetry of eddy currents only half of a single lamination has modeled. To model edge effects correctly a relatively fine mesh is needed in case of 3-D and I have used seven to twelve layered mesh along the thickness of lamination under consideration.

4.1 Boundary conditions

Unique field distribution solution within the lamination is obtained by setting the normal component of $\boldsymbol{B}$ on its boundaries along with the normal component of $\boldsymbol{J}$ to zero [22]. This method is later applied on induction machine lamination model for eddy current calculation [7]. The application of the normal component of $\boldsymbol{B}$ on the boundary is equivalent to specifying the tangential component of $\boldsymbol{A}$ which forms the basis of calculation as we are using edge elements instead of nodal elements for 3-D computation. To apply zero normal current density $\boldsymbol{J}_n$ on the sheet surface, the scalar potential V was set as free. To force average magnetic flux density as same as 2-D, the tangential component of $\boldsymbol{A}$ on the boundaries along the lamination thickness is extrapolated from the 2-D vector potential and assumed to be constant along the thickness. Further to provide magnetic insulation at top and bottom surfaces, tangential vector potential ($\boldsymbol{A} \times \boldsymbol{n}$) is set to zero on these boundaries. The boundary conditions are presented in figure 4.1.

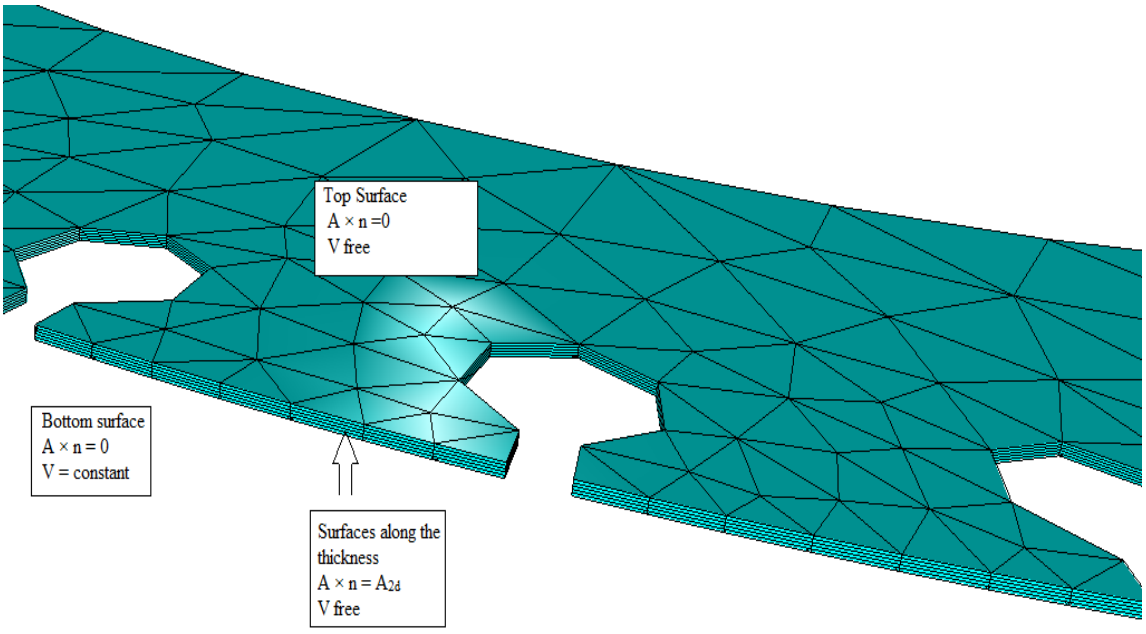

Figure 4.1 Boundary condition for AVA formulation

4.2 Homogeneous flux density case

A simple example of homogeneous flux density distribution was modelled in 3-D with similar conditions as described for 1-D case. A cuboid of area 20 mm×20 mm was considered with varying thickness from 0.2 mm to 2.5 mm. Magnetic flux density was considered in y direction and varying sinusoidally with respect to time.

$$\boldsymbol{B} = 1.5\sin(2\pi ft)\boldsymbol{u}_y . \tag{4.1}$$

To achieve such a flux distribution, z component of magnetic vector potential along the thickness of the lamination was defined as Dirichlet condition. The x and y components of magnetic vector potential along the lamination thickness were set free. Moreover the magnetic insulation condition was set on the top and bottom surfaces as shown in ELMER solver file attached in appendix A. I have used both cases of linear and non-linear material with relative permeability of 1000 and single value BH curve of figure 3.1, respectively. A time and position dependent z component of vector potential is presented in equation 4.2.

$$\boldsymbol{A}_{z3D} = -1.5x * \sin(2\pi ft)\boldsymbol{u}_z \tag{4.2}$$

The homogeneous distribution of magnetic flux density has been observed in case of linear and nonlinear material. Further two hundred time steps per period were considered using time discretization method BDF of order one. The peak flux density without any conductivity in a lamination is shown in figure 4.2.

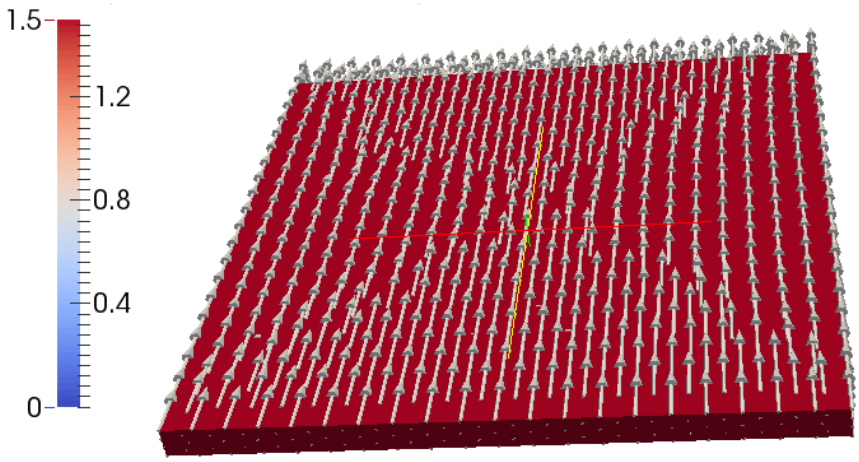

Figure 4.2 Homogeneous flux density distribution

At the conductivity of 8×10^6 S/m eddy currents are produced in the lamination due to sinusoidal time varying magnetic flux density. As the flux density was pointing in the *y* direction, the corresponding eddy currents can be seen in *x* direction to oppose this change. Further the zero current density at the middle of lamination was forced by applying constant scalar potential and seems to hold nicely. The normal component of magnetic flux density and current density at the top surface was also analyzed in post-processing and recorded as negligible compared to corresponding lamination plane values. The eddy currents are represented by figure 4.3.

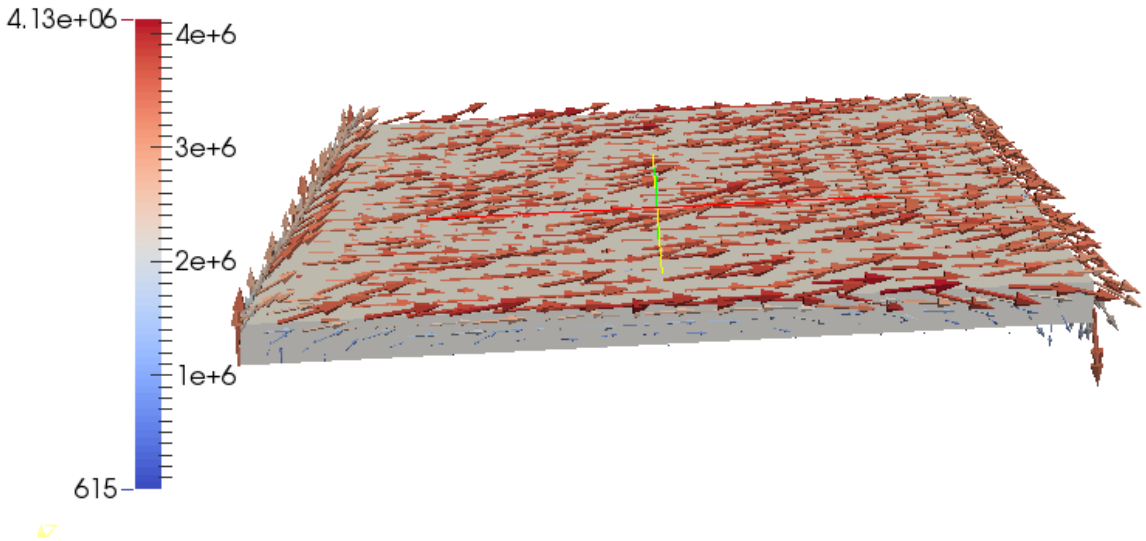

Figure 4.3 Eddy current density in homogeneous medium

The eddy current losses are calculated for two periods and to remove the effect of transients the second period was considered to analyze losses. Losses with linear material (relative permeability 1000) and nonlinear material are presented in tables 4.1 and 4.2 respectively. The difference between 1-D coupled 2-D model and 2-D coupled 1-D model is negligible upto lamination thickness 2 mm (w/d=10).

Table 4.1 Linear material with 50 Hz

Lamination thickness (mm)	***w/d***	**1-D Numerical (kW/m^3)**	**1-D Analytical (kW/m^3)**	**3-D (kW/m^3)**	**% Difference with respect to 1-D numerical**
0.5	40.0	18.59	18.50	22.10	18.91
0.65	30.8	31.41	31.25	37.20	18.42
1	20.0	74.29	73.73	75.25	1.29
1.5	13.3	166.47	163.32	161.99	-2.69
2	10.0	292.79	279.05	290.33	-0.84
2.25	8.9	343.26	341.99	318.80	-7.13
2.5	8.0	406.55	405.19	371.93	-8.52

Table 4.2 Nonlinear material with 50 Hz

Lamination thickness (mm)	***w/d***	**1-D Numerical (kW/m^3)**	**3-D (kW/m^3)**	**% Difference with respect to 1-D numerical**
0.5	40.0	19.30	22.22	15.12
0.65	30.8	33.46	37.75	12.80
1	20.0	83.31	82.65	-0.79
1.5	13.3	196.89	197.73	0.43
2	10.0	360.44	357.31	-0.87
2.25	8.9	460.78	442.81	-3.90
2.5	8.0	573.19	546.87	-4.59

Further, cases of higher frequencies are considered to analyze edge effects on eddy current losses. On the contrary to 50 Hz supply considerable amount of difference in results of 1-D and 3-D eddy current loss models have been observed below width/thickness ratio of 13. Nonlinear material with 1000 Hz and 5000 Hz supply frequency are represented in table 4.3 and 4.4 respectively.

Table 4.3 Nonlinear material with 1000 Hz

Lamination thickness (mm)	*w/d*	1-D Numerical (MW/m^3)	3-D (MW/m^3)	% Difference with respect to 1-D numerical
0.5	40.00	9.22	5.93	-35.71
1.5	13.33	84.21	80.62	-4.26
2	10.00	144.23	133.24	-7.62
2.25	8.89	178.75	162.18	-9.27
2.5	8.00	216.42	195.09	-9.86

Table 4.4 Nonlinear material with 5000 Hz

Lamination thickness (mm)	*w/d*	1-D Numerical (MW/m^3)	3-D (MW/m^3)	% Difference with respect to 1-D numerical
0.5	40.00	239.27	309.60	29.39
1.5	13.33	1852.30	1958.40	5.73
2	10.00	3167.30	2955.60	-6.68
2.25	8.89	3946.80	3641.70	-7.73
2.5	8.00	4800.60	4345.10	-9.49

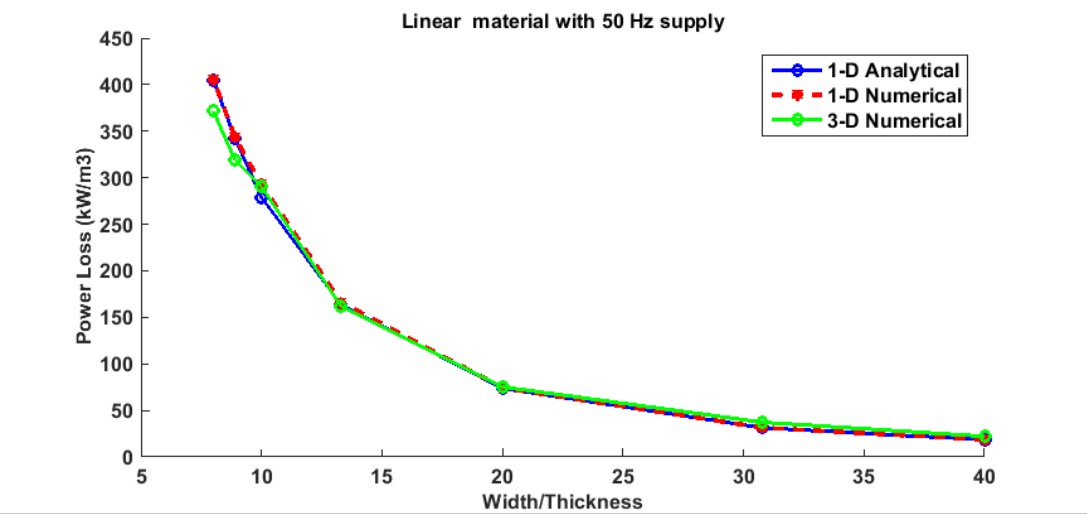

Figure 4.4 Eddy current loss at supply frequency 50 Hz with linear material

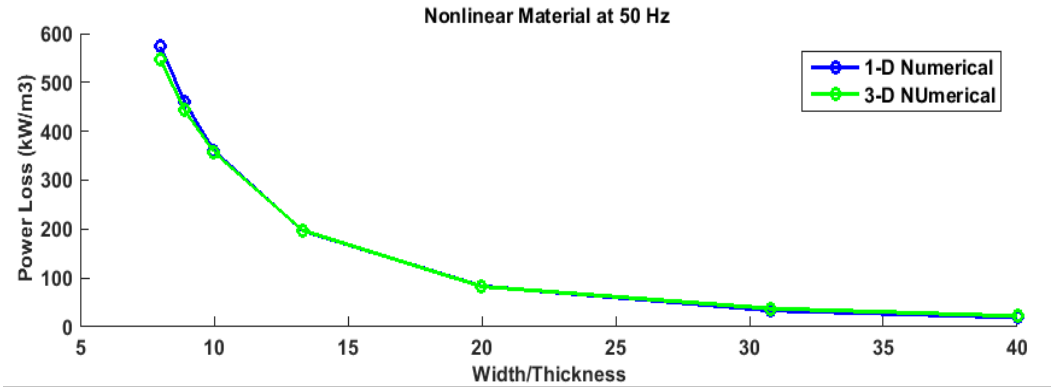

Figure 4.5 Eddy current loss at supply frequency 50 Hz with nonlinear material

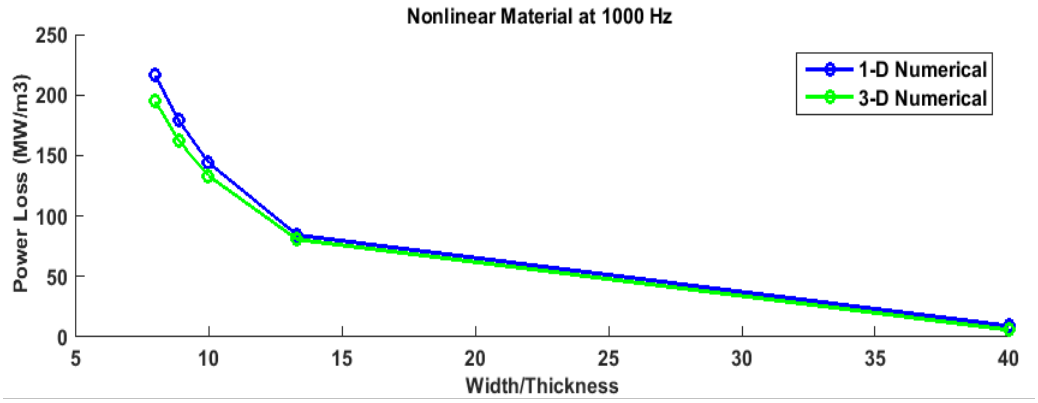

Figure 4.6 Eddy current loss at frequency 1000 Hz

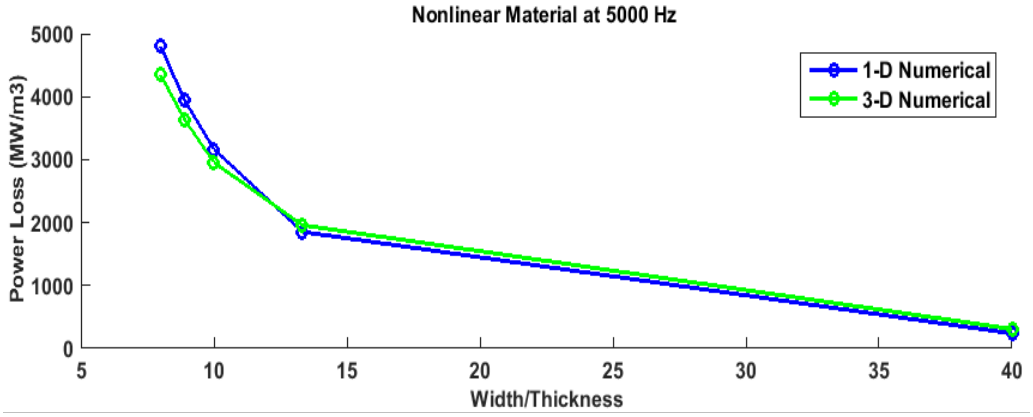

Figure 4.7 Eddy current loss at frequency 5000 Hz

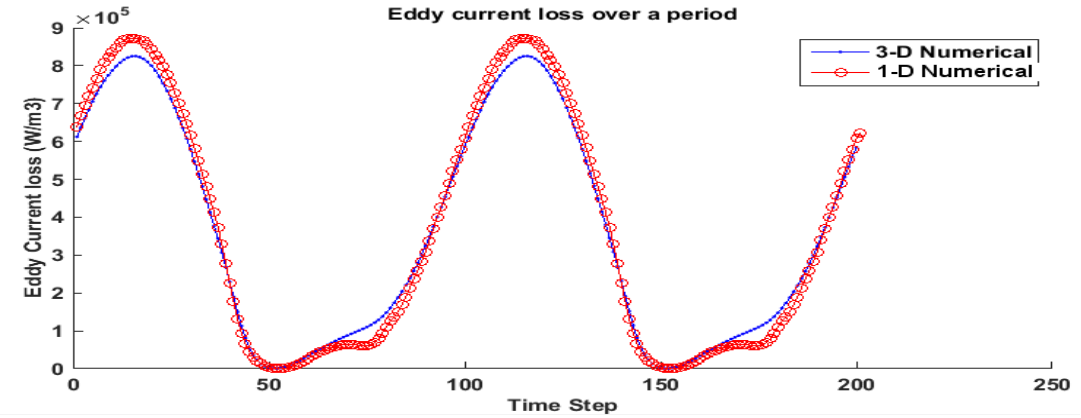

Figure 4.8 Eddy current loss comparison over a period of 200 time steps

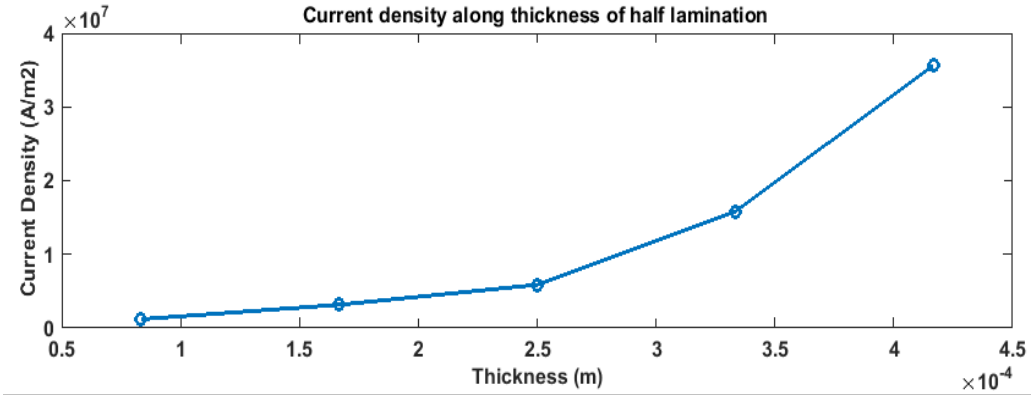

Figure 4.9 Current density along the lamination thickness

As the result of 0.5 mm lamination thickness has shown abnormally higher value in eddy current losses, a more refined mesh has been analyzed to check the possible anomalies due to mesh quality.

Table 4.5 Mesh troubleshooting

Parameters	**Mesh(a)**	**Mesh(b)**
Thickness layers	6	5
Nodes	24632	47726
Elements	82247	240300
1-D result power loss (kW/m^3)	19.30	19.30
3-D result power loss (kW/m^3)	22.21	20.48
% difference with respect to 1-D numerical	15.11	6.15

Analyzing the results shown in table 4.5, it was concluded that by improving 3-D mesh quality a closer result to 2-D loss model can be achieved. However due to large computation time of 0.5 mm lamination case, further mesh refinement was considered complex task for this thesis.

From the results of 50 Hz, 1000 Hz and 5000 Hz test cases, it can be observed that 1-D coupled 2-D model overestimates eddy current losses due to edge effects. A comparative analysis of effect of frequency with increasing width to thickness ratio is presented in table 4.6. Clearly an incremental effect due to edges can be seen at higher frequencies.

Table 4.6 Effect of frequency

w/d	**% Difference with respect to 1-D numerical at 50 Hz**	**% Difference with respect to 1-D numerical at 1000 Hz**
13.33	0.43	-4.3
10	-0.87	-7.6
9.00	-3.9	-9.3
8.00	-4.6	-9.8

4.3 Rotor pole of salient pole synchronous machine

The geometry of machine rotor pole has been prepared in GMSH after extracting the part of whole 2-D machine mesh which deals with a pole. Here we have to note that whole machine is simulated in 2-D FEM software FCSMEK and solution is then applied to excite the 3-D model of pole at the boundaries. Details of boundary conditions are shown in figure (4.1). The whole 3-D simulation process can be seen in the flowchart below

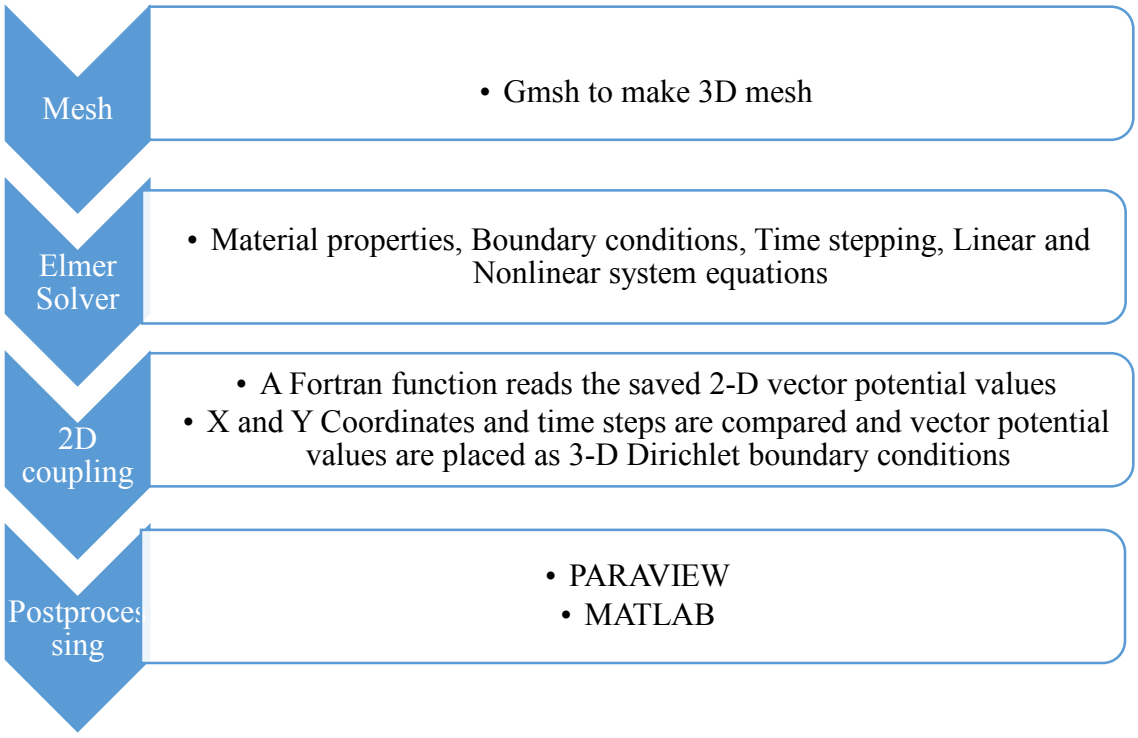

From the results of homogeneous case it is observed that when width to thickness ratio is below 13 and frequency of magnetic flux density is in kHz range a considerable amount of difference between 2-D and 3-D eddy current losses exist. Though it is not possible to arrive at a uniform width to thickness ratio in case of salient pole rotor lamination, a lower *w/d* ratio can be seen at the area between the damper bars as presented in figure 4.10.

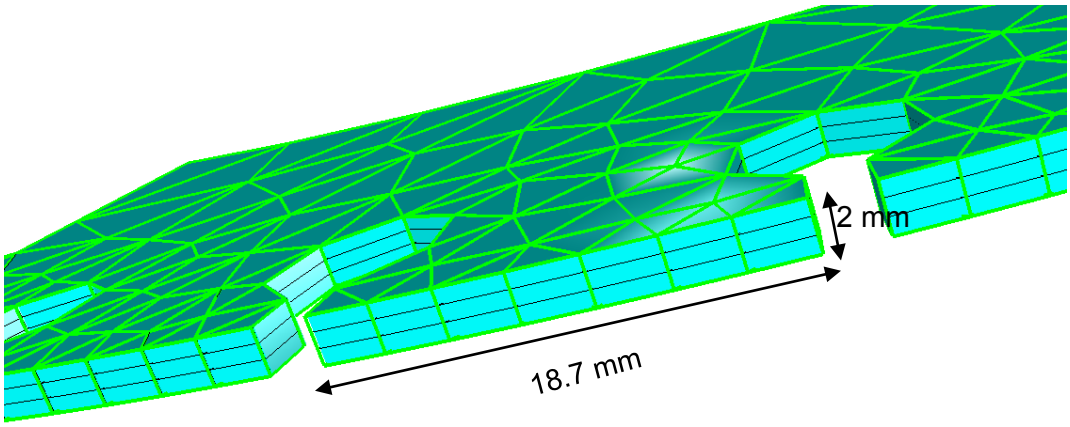

Figure 4.10 3-D model of rotor pole

After simulation at a particular time step the distribution of magnetic flux density in 3-D case has been observed (figure no. 4.11) and compared with 2-D FEM (figure no. 3.3) and a satisfactory similarity has been observed.

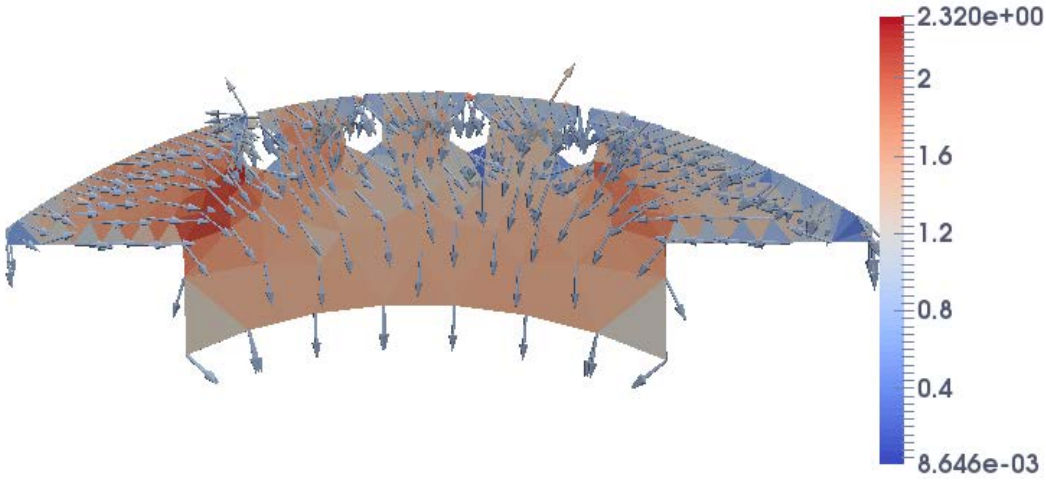

Figure 4.11 Flux density distribution in 3-D rotor pole geometry

The eddy currents will only present at rotor pole area along the air gap due to varying flux density because of slot harmonics as presented in figure 4.12.

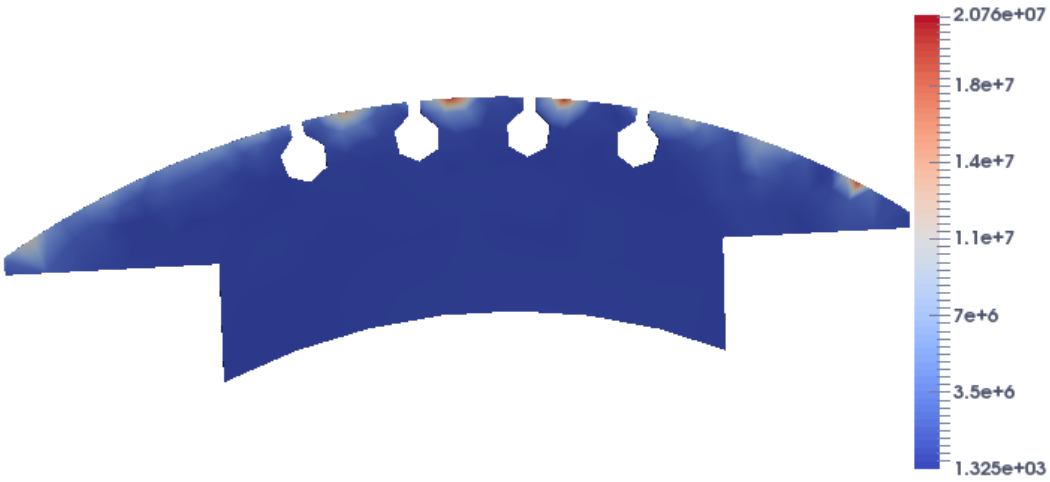

Figure 4.12 Spatial distribution of eddy current density in rotor pole

At first possibility of applying vector potential values from 2-D field solution on the same mesh as 2-D configuration has been analyzed. However the requirement of having enough mesh layers along the lamination thickness (more than five) for providing zero tangential current density at the middle of lamination resulted in low quality mesh elements. Therefore denser meshes have been analyzed in 3-D case. As application of a denser mesh in 2-D FEM software FCSMEK was relatively tedious task, linearly interpolated vector potential values were applied at the boundaries of denser 3-D meshes. Further to avoid transients, first quarter of supply frequency cycle has been ramped, as 2000 thousand time steps were considered per cycle in 2-D FEM calculation, a total of 2500 time steps were analyzed and average eddy current losses were considered after ramping. The main results for the rotor pole with lamination thickness 2 mm are shown in table 4.7.

Table 4.7 Rotor pole results with different meshes

Parameters	Mesh 1	Mesh 2	Mesh 3	Mesh 4
Number of nodes at boundary	120	240	480	960
Total number of elements	1,809	28,650	149,478	851,880
Number of mesh layers along thickness	6	6	8	10
2-D eddy current loss (W)	1894	1894	1894	1894
3-D eddy current loss (W)	1407	1980	1730	1867
Percentage difference with 2-D	-25.7	4.5	-8.63	-1.42

As an initial run, rotor case with lower lamination thickness has been performed, however results are found unreliable due to poor mesh quality. A relatively higher number of mesh elements are required for lower lamination thicknesses as compared to the case listed in mesh 4. Due to time constrains and considering high computational burden, the analysis of lower thicknesses is considered out of the scope of this thesis work.

However the result of mesh 4 considered to be credible for 2 mm lamination thickness case and the difference between two and three dimensional FEM are considered as representation of edge effects.

5. Conclusion and Discussion

Finite element analysis is performed for steel laminations across wide range of thicknesses with 1-D coupled 2-D and 2-D coupled 3-D eddy current loss models. Two separate cases, one with homogeneous flux density and another with non-homogeneous flux density were studied and results are compared. Moreover to reduce the computational burden of simulating the whole machine in 3-D, a 2-D coupled analysis is presented in this thesis work and boundary conditions are excited with the 2-D FEM results in case of rotor pole lamination of salient pole synchronous machine. The objective of this comparative study between different dimensional lamination models was to analyze the edge effects in calculation of eddy current losses. As the traditionally available 1-D coupled 2-D eddy current loss model neglects the edge effects, the corresponding difference with 3-D model was seen as edge effects.

As part of research work first one dimensional simple eddy current loss model was considered across generally available laminations. The results are nearly same in comparison to the obtained losses from classical analytical eddy current expressions for linear material. Then the average flux density was supplied to 3-D model with excitation of vector potential at the boundaries. The results in study case were found in good resemblance and uniform distribution of flux across the studied 3-D model was observed. Analyzing the results, it was found that edge effects create greater influence with increasing thickness and proves the thought of the increasing eddy current loss difference with 3-D in comparison with 1-D coupled 2-D models. However challenges have been observed in creating quality mesh with lower thicknesses such as 0.2 mm and 0.5 mm. The abnormalities in 3-D loss calculation of these lamination results are explained with a test case of highly dense mesh of 0.5 mm and results show a relatively better agreement. Based on this result it was concluded that very high number of elements (more than 0.3 million) are needed in order to get credible result and parallelization technique should be used for computation.

Further, as nowadays variable frequency drives are extensively used for the machine supply purpose, different supply frequencies such as 1000 Hz and 5000 Hz were tested with given nonlinear steel laminations. As a result it was concluded that there is net decrement in 3-D modeled eddy current loss as compared to 2-D/1-D loss and this difference is dependent on lamination thickness and frequency with major effect on lamination thickness 1 mm (w/d<13) onwards and frequency greater than 1 kHz.

Finally to study the effects in a nonhomogeneous flux distribution case a 150 kVA four pole salient pole synchronous machine was considered. The selection of this specific machine enables us to analyze relatively thick laminations such as a thickness of 2 mm to study edge effects. The whole machine was first simulated by in-house 2-D finite

element software “FCSMEK” and eddy current losses are calculated as per the 1-D coupled 2-D loss model. The 2-D vector potential values are saved for the boundary nodes of a rotor pole. Specific consideration has been given to mesh generation in 3-D for this specific case as per the experience from homogeneous test cases. Four different meshes are simulated and obtained 2-D vector potential values are linearly interpolated to provide boundary conditions for 3-D model. As part of the result the finest mesh was considered to be good enough for loss comparison and shows 1.4% decrement in eddy current losses as compared to 2-D. However a uniform *w/d* ratio cannot be assigned for the given lamination structure and only the regions between damper bars have relatively lower *w/d* around 9.

From the analyzed cases of homogeneous and nonhomogeneous magnetic flux density, it can be concluded that for most of the practical cases in electrical machines ($w/d > 10$ and frequency in kHz range), the 1-D coupled 2-D method is good enough for eddy current loss calculation. Further, for the salient pole synchronous machine a case with PWM supply and full load should give a bit higher difference between the studied loss models due to increased eddy current losses and corresponding edge effects. However from result of homogeneous test case (nonlinear case of 2 mm thickness with 1kHz frequency) this difference should be less than 7%.

As part of future work on this topic, I will suggest to use high number of elements at lower lamination thicknesses and use of parallel computing in order to reduce the high time requirement of computation. Possibility of modelling air near the edges will also help in looking at the fringing effect of flux. I have also tried to observe the surface magnetic field intensity, a comparative study shows that thinner lamination shows comparatively better resemblance with 1-D model. Therefore it may be possible to do a more detailed study of surface field intensity. Moreover, during this work, focus was to apply average flux density to lamination, however a better result may be achieved if surface vector potential values can be applied along the lamination. In this thesis magnetic insulation conditions ($\boldsymbol{A} \times \boldsymbol{n} = 0$) have been applied to surfaces along the lamination surface. I have tried to use surface magnetic flux intensity as boundary condition along the lamination and as a result the zero normal flux density condition was automatically satisfied [Appendix D]. However the field strength is discontinuous in 2-D nonhomogeneous case and can only be approximated, for example by weighted average of elements area containing a node; this possibility can also be checked. Due to time constrain I have examined the case of rotor lamination thickness of 2 mm, however cases of lamination thicknesses 1 mm, 0.5 mm and 0.2 mm should show better compliance with 1-D coupled 2-D model.

References

[1] European commission guidelines on eco design requirements for electric motors, 2014.

[2] L. M. Bash, and D. S. Pekarek, "Modeling of salient-pole wound-rotor synchronous machines for population-based design," *IEEE Trans. Energy Convers.*, vol. 26, no. 2, pp. 381–392, 2011.

[3] A. H. Toliyat, and A. N. Al-Nuaim, "Simulation and detection of dynamic air-gap eccentricity in salient-pole synchronous machine," IEEE *Trans. Ind. Appl.*, vol. 35, no. 1, pp. 86–93, 1999.

[4] G. Dajaku, and D.Gerling, "Air gap flux density characteristics of salient pole synchronous permanent-magnet machines," *IEEE Trans. Magn.*, vol. 48, no. 7, pp. 2196–2204, 2012.

[5] D. Albertz, and G. Henneber, "Calculation of 3-D eddy current fields using both electric and magnetic vector potential in conducting regions," *IEEE Trans. Magn.*, vol. 34, no. 5, pp. 2644–2647, 1998.

[6] O. Biro, "Edge element formulations of eddy current problems," *Comput. Methods in Appl. M.*, vol. 169, no. 3-4, pp. 391–405, 1999.

[7] P. Handgruber, A. Stermecki, O. Biro, A. Belahcen, and E. Dlala, "3-D eddy current analysis in steel laminations of electrical machines as a contribution for improved iron loss modeling," *IEEE Trans. Ind. Appl.,* vol. 49, no. 5, pp. 2044–2052, 2013.

[8] C. P. Steinmetz, "On the law of hysteresis," *Am. Inst. Electr. Eng. Trans.*, vol. 9, pp. 3–64, 1892.

[9] J. Gyselinck, and P. Dular, "Calculation of eddy currents and associated losses in electrical steel laminations," *IEEE Trans. Magn.*,vol. 35, no. 3, pp. 1191–1194, 1999.

[10] A. Arkkio, "Analysis of induction motors based on the numerical solution of the magnetic field and circuit equations," ISBN 951-22-6076-X, 1987.

[11] Elmer solver manual chapter 6.

[12] J. P. A. Bastos, and N. Ida, "Electromagnetics and calculation of fields," 2nd ed. Springer, 1997.

[13] J. C. Nédélec, "Mixed finite elements in 3R," Numeric. Math., vol. 35, pp. 315–341, 1980.

[14] A. Bossavit, "A rationale for edge elements in 3-D fields computations," *IEEE Trans. Magn.*, vol. 24, no. 1, pp. 74–79, 1998.

[15] J. S.Wang, and N. Ida, "Curvilinear and higher order edge finite elements in electromagnetic field computation," *IEEE Trans. Magn.*, vol. 29, no. 1, pp. 1491–1494, 1992.

[16] J. P. Webb, "Edge elements and what they can do for you," *IEEE Trans. Magn.,* vol. 29, no. 2, pp. 1460–1465, 1993.

[17] O. Bottauscio, M. Chiampi, and D. Chiarabaglio, "Advanced model of laminated magnetic cores for two-dimensional field analysis," *IEEE Trans. Magn.,* vol. 36, no. 3, pp. 561–573, 2000.

[18] P. Rasilo, "Finite-element modeling and calorimetric measurement of core losses in frequency converter supplied synchronous machine," Doctoral Dissertation, Aalto University, 2012.

[19] URL: https://www.csc.fi/web/elmer.

[20] URL: http://www.nic.funet.fi/pub/sci/physics/elmer/doc/ElmerModelsManual.pdf, chapter 14.

[21] URL: http://www.paraview.org/.

[22] O. Biro, K. Preis, and I. Ticar, "A FEM method for eddy current analysis in laminated media," *COMPEL*: *Int. J. for Compu. Math. Elect. Electron. Eng.*, vol. 24, no. 1, pp. 241–248, 2005.

Appendix A

Solver Input File for 3-D computation of rotor pole lamination

```
Header
  CHECK KEYWORDS Warn
  ! Mesh file name
  Mesh DB "singlesplitrotor"
  Include Path ""
  Results Directory ""
End

Simulation
  Max Output Level = 9
  Coordinate System = Cartesian
  !Coordinate Scaling = 0.001
  !Extruded Mesh Levels = Integer 4
  Simulation Type = transient
  ! Defining the time stepping method and parameters
  Timestepping Method = BDF
  BDF Order = 1
  Timestep Sizes = 1e-5
  Timestep Intervals = 2500
  Steady State Max Iterations = 1
  Output Intervals = 1
End

Body 1
  Target Bodies(1) = 1
  Name = "Body 1"
  Equation = 1
  Material = 1
End

!solver for filed computation
Solver 1
  Exec Solver = Always
  Equation = "MGDynamics"
  Variable = "AV"
  Procedure = "MagnetoDynamics" "WhitneyAVSolver"
  Fix Input Current Density = Logical false
  Use Piola Transform = Logical True
  Use Tree Gauge = Logical False
  Steady State Convergence Tolerance = 1.0e-5
  Newton-Raphson iteration = logical true
  Nonlinear System Convergence Tolerance = 1.0e-6
  Nonlinear System Max Iterations = 100
  Nonlinear System Newton After Iterations = 3
  Nonlinear System Newton After Tolerance = 1.0e-3
```

```
  Nonlinear System Relaxation Factor = 1
  Linear System Solver = Iterative
  Linear System Preconditioning = none
  Linear System Iterative Method = gcr
  Linear System Residual Output = 20
  Linear System Max Iterations = 2500
  Linear System GCR Restart = 600
  Linear System Convergence Tolerance = 1e-9
  Linear System Abort Not Converged = False
  Steady State Convergence Tolerance = 1e-9
  Linear System Normwise Backward Error = Logical true
  Edge Basis = Logical True
  Apply Mortar BCs = Logical False
End

!Solver for deriving field quantities from FEM
Solver 2
  Exec Solver = always
  Equation = "MGDynamicsCalc"
  Procedure = "MagnetoDynamics" "MagnetoDynamicsCalcFields"
  Linear System Symmetric = True
  Potential Variable = String "AV"
  Use Piola Transform = Logical True
  Calculate Current Density = Logical True
  Calculate Electric Field = Logical False
  Calculate Magnetic Field Strength = Logical false
  Calculate Magnetic Vector Potential = Logical True
  Calculate Magnetic Flux Density = Logical True
  Calculate Field Energy = Logical False
  Calculate Elemental Fields = Logical True
  Linear System Solver = "Iterative"
  Linear System Preconditioning = ilu0
  Linear System Residual Output = 0
  Linear System Max Iterations = 5000
  Linear System Iterative Method = gcr
  Linear System Convergence Tolerance = 1.0e-8
  Edge basis = Logical True
End


!Solver for saving eddy current loss at each time step
Solver 3
 Exec Solver = After Timestep
 Equation = SaveScalars
 Procedure = "SaveData" "SaveScalars"
 Filename = "Data.dat"
 Output Directory = splitrotor
End

Equation 1
  Name = "ModelDomain"
  Active Solvers(3) = 1 2 3
```

```
End



!material specification and sinlge value BH curve definition
Material 1
  Name = "Iron"
Electric Conductivity = real 7.85e6
   H-B Curve(182,2) = Real
   INCLUDE bhcurvenonlinear.txt
End

!application of 2-D vector potential values
Boundary Condition 1
  Target boundaries(1) = 1
  AV {e} 3 = Variable coordinate,time
    Real Procedure "coupling.so" "coordinate"
End

!Boundary condition for Bottom Surface
Boundary Condition 2
  Target boundaries(1) =3
  AV {e} = Real 0.0
  AV = Real 1.0
End

!Boundary condition for Top Surface
Boundary Condition 3
  Target boundaries(1) =2
  AV {e} = Real 0.0
End
```

Appendix B

2-D Coupling by User Function in FORTRAN 90

```
FUNCTION coordinate (Model, n, A) Result(coordu)
USE DefUtils
IMPLICIT None
TYPE(Model_t) :: Model
TYPE(Solver_t):: Solver


TYPE(Nodes_t), POINTER:: ElementNodes
TYPE(Mesh_t), POINTER :: Mesh

Logical, save :: FirstTime = .True.


Integer :: i, n

REAL(KIND=dp):: coordu, diffx
Real(KIND=dp) :: A(4)
Real(KIND=dp), DIMENSION(1200000,4),SAVE:: AZ
character(512) :: line
LOGICAL, SAVE :: First_Time = .True.
! Loading a file with xy coordinates of boundary nodes, time and respective
vector potential value
IF (First_Time) THEN
    First_Time = .False.
OPEN (10, FILE="Adoublerefeinedwithtime.txt",STATUS="OLD",ACTION="READ")
DO i = 1,1200000
READ(10,*) AZ(i,1),AZ(i,2),AZ(i,3),AZ(i,4)
END DO
CLOSE(10)
END IF

  Mesh => GetMesh()
  ElementNodes => Mesh % Nodes
! Comparing the 3-D boundary node A(4) coordinates and time and sending the 2-
D vector potential value AZ (4) as coordu to Dirichlet condition in sif
DO i = 1 , 1200000
  diffx = SQRT((A(1)- AZ(i,1))* (A(1)- AZ(i,1))+(A(2)- AZ(i,2)) *(A(2)-
AZ(i,2))+(A(4)- AZ(i,3)) *(A(4)- AZ(i,3)))
IF (diffx.LT. 0.00000001 )then
        coordu = AZ(i,4)
exit
ENDIF
END DO


END FUNCTION coordinate
```

Appendix C

Making GMSH geometry as per refined mesh after 2-D mesh element splitting

```
M = dlmread('mesh1.nodes');

 % reading 2-D splitted mesh files in elmer grid format
nodenumber= M(1:3137,1);
xcord=M(1:3137,3);
ycord=M(1:3137,4);

n=1;
i= [8:-1:1 9 49:-1:43 118 149 179 180 181:198 157 155 153 152 151
154 156 199:206 164 162 160 159 158 161 163 207:214 171 169 167 166
165 168 170 215:222 178 176 174 173 172 175 177 223:242 150 148 91:-
1:85 27 8];

% finding the new boundary nodes in order

for j=1:120
      boundarynode(n)=i(j);
       n=n+1;
for s=1:3
     x=(xcord(i(j))*(4-s)+xcord(i(j+1))*s)/4;
     y=(ycord(i(j))*(4-s)+ycord(i(j+1))*s)/4;

for k=1:3137
        diffx= sqrt((xcord(k)-x)*(xcord(k)-x));
        diffy= sqrt((ycord(k)-y)*(ycord(k)-y));
if (diffx<1e-6)&&(diffy<1e-6)
            boundarynode(n)=k;
            n=n+1;
end
end
end
end

%writing new geo file for GMSH
fid = fopen('doublesplitrotor.geo','w')
t=0;
p=1;
for x=1:480
fprintf(fid,'Point(%d) =
{%f,%f,%d,%d};\n',x,xcord(boundarynode(1,x)),ycord(boundarynode(1,x)
),t,p);
end
for y=1:479
fprintf(fid,'Line(%d) = {%d,%d};\n',y,y,y+1);
end
fprintf(fid,'Line(%d) = {%d,%d};\n',y+1,y+1,1);
fclose('all')
```

Appendix D

Coupling of 1-D surface field intensity ($\boldsymbol{H}_s$) with 3-D model

- Analytical eddy current loss = 279.05 kW/ m^3
- Eddy current loss with $\boldsymbol{H}_s$ as boundary condition = 281.64 kW/m^3
- Eddy current loss without $\boldsymbol{H}_s$ as boundary condition = 291.59kW/ m^3

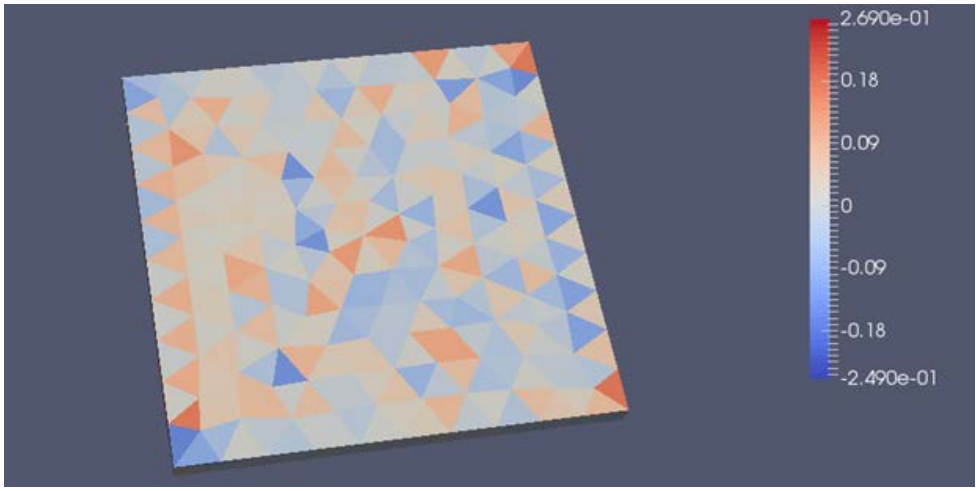

Figure Normal magnetic flux density distribution